JACS
JOURNAL OF THE AMERICAN CHEMICAL SOCIETY
pubs.acs.org/JACS
Article

Cation Modifies Interfacial Water Structures on Platinum during Alkaline Hydrogen Electrocatalysis

Pengtao Xu,*[,∇] Ruiyu Wang,[∇] Haojian Zhang, Vincenzo Carnevale, Eric Borguet, and Jin Suntivich*

Cite This: https://doi.org/10.1021/jacs.3c09128
Read Online
ACCESS | Metrics & More | Article Recommendations | Supporting Information

ABSTRACT: The molecular details of an electrocatalytic interface play an essential role in the production of sustainable fuels and value-added chemicals. Many electrochemical reactions exhibit strong cation-dependent activities, but how cations affect reaction kinetics is still elusive. We report the effect of cations (K^+, Li^+, and Ba^{2+}) on the interfacial water structure using second-harmonic generation (SHG) and classical molecular dynamics (MD) simulation. The second- ($\chi^{(2)}_{H_2O}$) and third-order ($\chi^{(3)}_{H_2O}$) optical susceptibilities of water on Pt are smaller in the presence of Ba^{2+} compared to those of K^+, suggesting that cations can affect the interfacial water orientation. MD simulation reproduces experimental SHG observations and further shows that the competition between cation hydration and interfacial water alignment governs the net water orientation. The impact of cations on interfacial water supports a cation hydration-mediated mechanism for hydrogen electrocatalysis; i.e., the reaction occurs via water dissociation followed by cation-assisted hydroxide/water exchange on Pt. Our study highlights the role of interfacial water in electrocatalysis and how innocent additives (such as cations) can affect the local electrochemical environment.

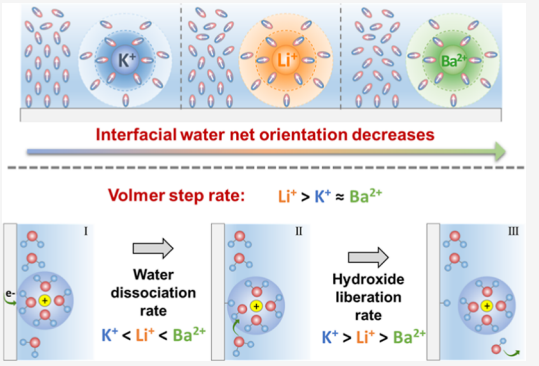

Downloaded via CORNELL UNIV on January 29, 2024 at 20:46:37 (UTC).
See https://pubs.acs.org/sharingguidelines for options on how to legitimately share published articles.

INTRODUCTION

Electrochemistry occurs through the synergistic interaction between a reactant and an electrode surface. Tuning this interaction has tremendously progressed our ability to design top-performing electrocatalysts.[1] Recently, the catalyst−electrolyte interaction has emerged as an important factor in controlling the electrode−reactant interaction.[2−5] An example is alkaline hydrogen evolution reaction (HER), where the cations in the order of Cs^+, Rb^+, K^+, Na^+, and Li^+ can increase the reaction kinetics.[6,7] A similar correlation between reaction rate and cation identity has also been reported for methanol oxidation reaction, oxygen reduction reaction,[8] water oxidation reaction,[9] and carbon dioxide reduction reaction.[10−12] The goal of this work is to understand the origin of the cation effect of alkaline HER using nonlinear spectroscopy and classical molecular dynamics (MD) simulations.

The impact of alkaline cations on interfacial water, which also functions as a reactant in the alkaline HER, is a subject of intense debate. Liu et al.[7] rationalized the effect of Li^+ in Pt alkaline HER through a hard−soft acid−base interaction, where hydrated Li^+ can more effectively than K^+ facilitate the OH desorption, which the authors assigned as the rate-limiting step. Alternatively, Huang et al.[6] proposed that weakly hydrated cations could alter the interfacial water structures in a way that increased the water reorganization energy and HER's entropic barrier. A recent study from Monteiro et al.[13] ascribed the cation effect to a site-blocking phenomenon, where the enrichment of weakly hydrated alkali cations like Cs^+ hindered water access to the electrode surface. While details vary, all of the above theories highlight the significance of interfacial water structures in alkaline HER.

Resolving the molecular details of interfacial cation−water interactions is challenging. A study using surface-enhanced infrared absorption spectroscopy[6] reported that cations of strong solvation promoted the formation of a hydrogen-bonded interfacial water network. However, another report using surface-enhanced Raman spectroscopy[14] found that the ability of water to form hydrogen bonding decreases when it is coordinated to cations, probably due to unfavorable molecular configurations as revealed by previous experimental and computational results.[15,16] These conflicting results highlight the difficulty in understanding the effect of cation on the water structure at electrochemical interfaces.

In this work, we use a combination of phase-sensitive second-harmonic-generation (PS-SHG) and classical MD simulation to analyze the effect of cations (Ba^{2+}, Li^+, and K^+) on interfacial water structures. As a probe of interfacial

Received: August 21, 2023
Revised: December 27, 2023
Accepted: December 28, 2023
Published: January 16, 2024

© 2024 American Chemical Society

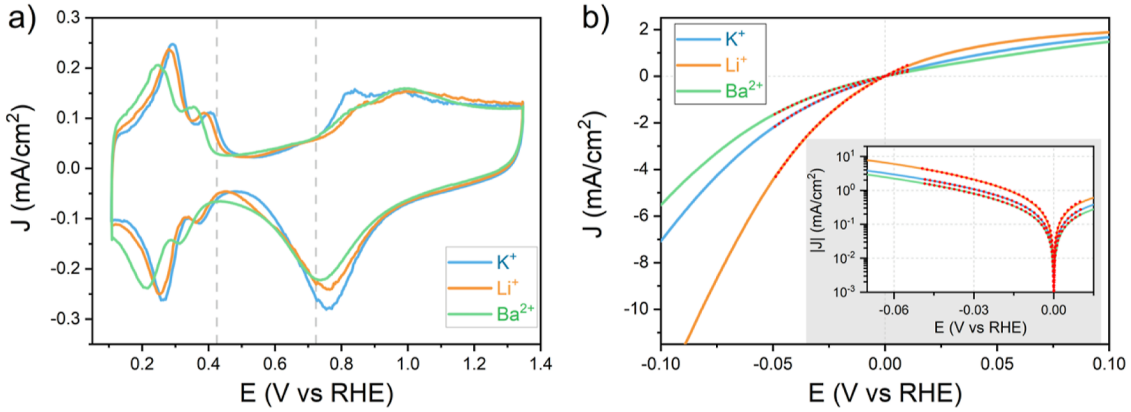

Figure 1. Effect of cations on Pt electrochemistry. (a) Cyclic voltammograms of a thin-film Pt electrode in different cation-containing electrolytes (saturated with Ar, scan rate: 200 mV/s). Gray dashed lines mark the potential window used for the SHG measurements. (b) Hydrogen electrochemistry of a Pt disk in different electrolytes (saturated with H_2, scan rate: 10 mV/s, rotation rate: 1600 rpm). The HER overpotential at -5 mA/cm^2 is 53.6 mV for Li^+, 82.2 mV for K^+, and 94.5 mV for Ba^{2+}. Inset: the same plot with the absolute current density on a log scale. Red dotted lines are the corresponding fits to the Butler–Volmer (eq 1) (see Table S1 for the full fitting results). All potentials are corrected for the voltage loss due to solution resistance. Electrolyte compositions: K^+, 0.1 M KOH; Li^+, 0.1 M LiOH; Ba^{2+}, 0.1 M KOH with 0.1 mM $Ba(OH)_2$.

effects,[17−20] SHG describes the conversion of two photons of the same frequency (ω) to one frequency-doubled photon (2ω) in a noncentrosymmetric medium (under the electric dipole approximation).[21] We have developed in situ phase-sensitive SHG (PS-SHG)[22] for tracking the interfacial electric field within the electrical double layer (EDL).[23] We show here that the SHG intensity from Pt–water interfaces decreases with cations of higher hydration energy. By decoupling the signals with contributions from the second- ($\chi^{(2)}_{H_2O}$) and third-order ($\chi^{(3)}_{H_2O}$) optical susceptibilities of water, we find that strongly hydrated cations such as Ba^{2+} reduce the net orientation of interfacial water molecules and their ability to align with the interfacial electric field.

To extend the understanding, MD simulations were carried out to reveal the atomic-level information on water structures and dynamics at interfaces, including the interaction among ions, water, and surfaces.[24,25] Atomic modeling of electrode surfaces using nonreactive, fixed charged model is challenging due to the lack of polarization of the ions and the surface, but this issue can be partially solved by scaling the charges.[26] For instance, classical MD simulations with scaled charged ions have been applied to study the stripping away of ions and the impact on the hydrogen bond network at water/metal surfaces.[6,27] Inspired by these findings, we have rescaled charges of ions by a factor of 0.95, as previously justified for the interaction between ions and charged water/metal surfaces.[28]

Our MD simulation reveals how the atomic details of interfacial water affect the SHG outcome; notably, the orientation of interfacial water molecules is the consequence of the balance between water–cation and water–electric-field interactions. This finding highlights how cations, in particular, their hydration rigidity, impact interfacial water structures. From our MD and SHG studies, our finding supports a cation-hydration-mediated mechanism, which could explain the cation-dependent H_{upd} (underpotential deposited hydrogen) positions and cation-dependent HER kinetics.

RESULTS AND DISCUSSION

Electrochemistry. The effect of cations on hydrogen underpotential deposition (H_{upd}) was evaluated by cyclic voltammetry (CV). As shown in Figure 1a, the H_{upd} potential shifted from K^+ to Li^+ to Ba^{2+} in a cathodic direction in the order of higher hydration energies, consistent with literature.[7,29,30] Using a Pt rotating disk electrode (RDE, Figure 1b), we measured the HER kinetics by linear sweep voltammetry. Replacing K^+ with Li^+ improved the HER kinetics, while the introduction of Ba^{2+} slightly worsened the reaction rate relative to K^+.

To quantify the observed kinetics, we fitted the polarization curves using the Butler–Volmer equation

$$J = J_0[e^{(1-\alpha)F\eta/RT} - e^{-\alpha F\eta/RT}] \quad (1)$$

where J_0 represents the exchange current density, α is the transfer coefficient, F is the Faraday constant, R is the universal gas constant, T is the temperature in Kelvin, and η is the overpotential. Figure 1b shows the Butler–Volmer fit (red dotted lines) to the experimental data (see Table S1 for fitting parameters).[31] The exchange current densities were 0.739, 1.318, and 0.534 mA/cm^2 for K^+, Li^+, and Ba^{2+}, respectively. As J_0 is associated with the rate constant, the analysis suggests that cations can affect the HER kinetics. The extracted Tafel slope trend from α, i.e., K^+ (92 mV/decade) and Li^+ (88 mV/decade), agrees qualitatively with the literature, which found a higher value for K^+ than Li^+.[6,13] The reported values in the literature are not exactly the same, likely a result of the potential range used for the Tafel slope fit.

In Situ SHG Measurements. To probe how cations affect exchange current densities, we characterize the cation effect using in situ SHG measurements. In our setup (Figure S2), the laser pulse interacts first with a LO (local oscillator) and then with the working electrode. This configuration generates nonlinear interferograms centered around 400 nm (Figure 2a) and bypasses the issue of optical dispersion in aqueous media, i.e., electrolyte.[22,23] Each interferogram was processed by Fourier transform[22] to retrieve the phase information (see Figure S3). The phase values were further corrected using a local reference phase based on sample position.[23]

Because the studied potential window (between the 2 gray dashed lines in Figure 1a) is within the double-layer region, the SHG response is predominantly a result of the water polarization (instead of electroadsorption) at the solid–liquid interface. Restricting the testing windows within the double-

https://doi.org/10.1021/jacs.3c09128
J. Am. Chem. Soc. XXXX, XXX, XXX−XXX

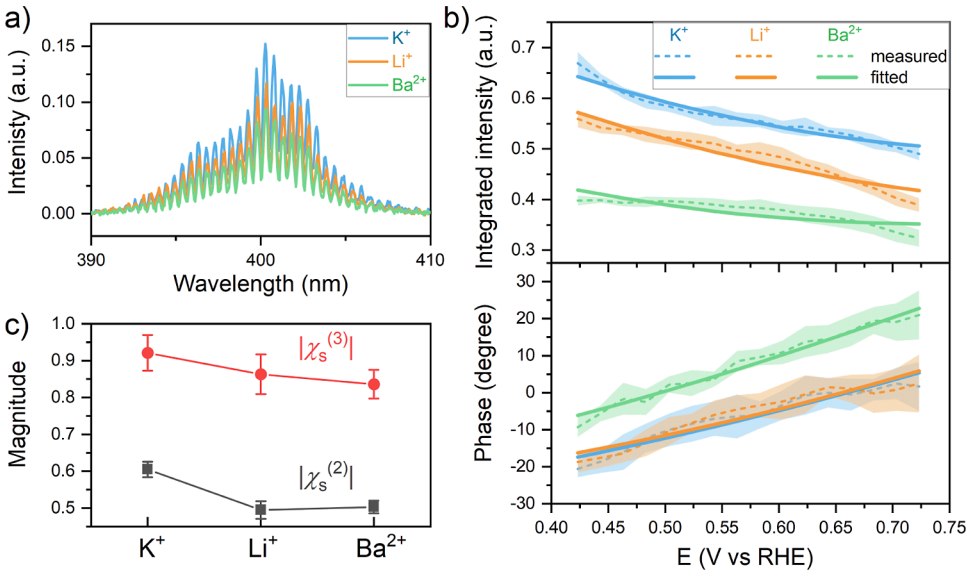

Figure 2. Effect of different cations on the SHG response of Pt−water interfaces. (a) Normalized SHG interferograms recorded in different cation-containing electrolytes at −0.425 V vs RHE (reversible hydrogen electrode). (b) Potential dependence of the SHG intensity and phase of the Pt−water interface in different cation-containing electrolytes. Scan rate: 20 mV/s. Dashed lines and the corresponding shaded regions represent the mean and standard deviation, respectively, averaged from three repeated measurements. Solid lines represent the best fit of eq 2 to the experimental data. (c) Fitted values (with fitting errors) of $|\chi_S^{(2)}|$ and $|\chi_S^{(3)}|$ with the data in (b). See Table S2 in the Supporting Information for full fitting parameters.

layer region also allows us to rationalize the origin of the SHG through a polarizable metal−dielectric model. In this scenario, the effective second-order optical susceptibility of the interface, $\chi_{eff}^{(2)}$, can be represented as

$$\chi_{eff}^{(2)} = \chi_S^{(2)} + \chi_S^{(3)}(E - E_{pzc}) \quad (2)$$

where $\chi_S^{(2)}$ is the interfacial second-order nonlinear susceptibility that is considered independent of the electric field in the EDL, and $\chi_S^{(3)}$ is the third-order nonlinear susceptibility describing the dc-field-induced nonlinear polarization of Pt surface electrons and interfacial water molecules. E is the applied potential to WE, and E_{pzc} is the potential of zero charge of Pt−water interfaces, which is 0.23 V vs SHE (or 0.997 V vs RHE under current experimental conditions) according to our previous study.[23] It is important to note that we cannot rule out the possibility that E_{pzc} could change with cations. We bring to the attention a recent double-layer measurement, which shows that the capacitance minimum depends on the cation identity, suggesting the need to further investigate a cation-dependent E_{pzc} in the future.[32]

The interfacial second-order nonlinear susceptibility contains information about the polarizability of the interface. We extract the susceptibility values by fitting eq 2 to the experimental data (Figure 2b, see Table S2 for fitting parameters.) Figure 2c compares the extracted $|\chi_S^{(2)}|$ and $|\chi_S^{(3)}|$ values of the Pt−water interface in the presence of different cations. $|\chi_S^{(2)}|$ with K^+ is larger than the values with Li^+ and with Ba^{2+}, and there is a clear decrease of $|\chi_S^{(3)}|$ in the order $K^+ > Li^+ > Ba^{2+}$.

To translate the susceptibility trend to molecular details, we first point out that $\chi_S^{(2)}$ and $\chi_S^{(3)}$ contain contributions from both the electrode and water at the interface

$$\chi_S^{(2)} = \chi_{Pt}^{(2)} + \chi_{H_2O}^{(2)} \quad (3)$$

$$\chi_S^{(3)} = \chi_{Pt}^{(3)} + \chi_{H_2O}^{(3)} \quad (4)$$

Conventional knowledge suggests that $\chi_{eff}^{(2)}$ is dominated by the metal's contribution (e.g., $\chi^{(2)}$ of Al is $\sim 10^{-18}$ m^2/V,[33] about five order-of-magnitude larger than that of water,[34] $\sim 10^{-23}$ m^2/V.) We have previously reported that $\chi_{Pt}^{(2)}$ is only about an order-of-magnitude larger than $\chi_{H_2O}^{(2)}$, while $\chi_{Pt}^{(3)}$ is comparable to $\chi_{H_2O}^{(3)}$ in magnitude.[23] Thus, while platinum is the larger contributor than water to SHG, the cation modification of $\chi_{H_2O}^{(2)}$ and $\chi_{H_2O}^{(3)}$ should still show its impact, especially considering that cations can affect the hydration structure in the Stern layer, e.g., at silica−water interfaces.[19,35] Similar observations have been reported by vibrational sum-frequency generation at air−water and lipid−water interfaces.[36−40] In this work, we assume that $\chi_{Pt}^{(2)}$ and $\chi_{Pt}^{(3)}$ remain constant in different cation-containing electrolytes and, therefore, we will analyze the SHG trend by attributing the observed change to the $\chi_{H_2O}^{(2)}$ and $\chi_{H_2O}^{(3)}$ terms in eqs 3 and 4.

Microscopically, $\chi_{H_2O}^{(2)}$ and $\chi_{H_2O}^{(3)}$ are related to hyperpolarizabilities, dipole moment, and water orientation.[41,42] Recent heterodyne-SHG studies[19,34,35] have attributed the origin of $\chi_{H_2O}^{(2)}$ and $\chi_{H_2O}^{(3)}$ to the water molecules in the Stern and diffuse layers, respectively. Considering that the selection rule of SHG requires noncentrosymmetric structures, in an ideal solvation shell, water reorients its negatively charged oxygen toward the cation, and the average $\chi_{H_2O}^{(2)}$ term of cation-bound water is zero due to symmetry. This symmetric interaction can be disturbed by interfacial polarization.[32] Cations with large hydration energy, e.g., Ba^{2+}, will resist this polarization as it takes more energy to disrupt the solvation structure, thereby leading to a smaller $\chi_{H_2O}^{(2)}$. Therefore, we conclude from Figure 2c that the cation hydration shells near the electrode surface (within the Stern layer) are more disrupted in "softer" K^+ than "harder" cations, e.g., Li^+ and Ba^{2+}.

https://doi.org/10.1021/jacs.3c09128
J. Am. Chem. Soc. XXXX, XXX, XXX−XXX

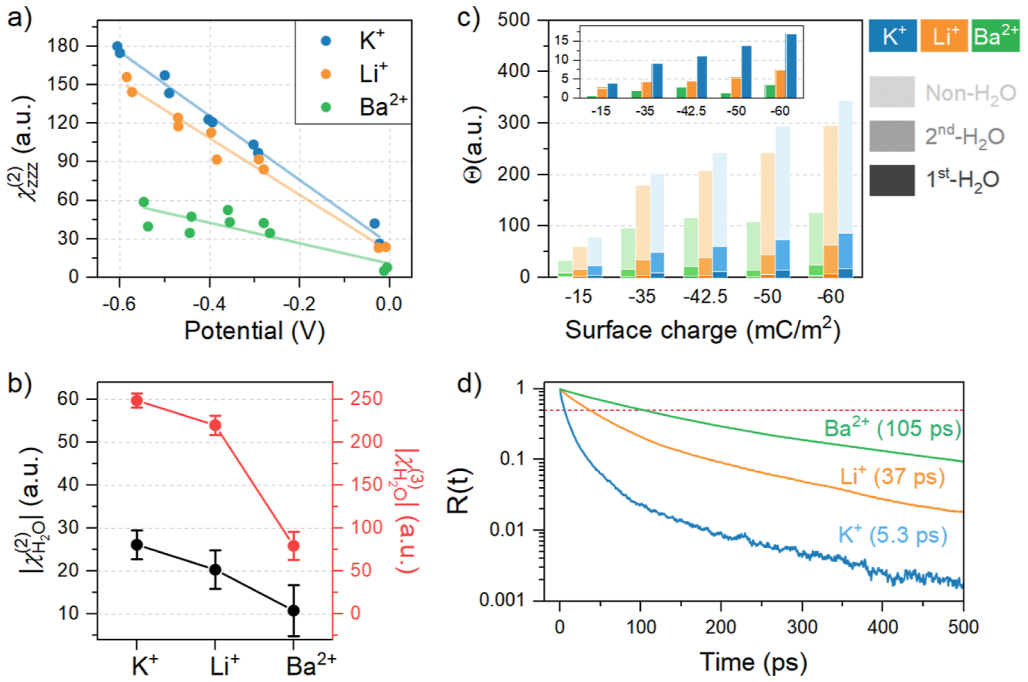

Figure 3. MD simulations of the structures and dynamics of interfacial water with different cations. (a) $\chi_{zzz}^{(2)}$ determined from simulations of water orientations as a function of cations and surface potential. Solid lines are the best fit of eq 2, with the fitted $\chi_S^{(2)}$ and $\chi_S^{(3)}$values (represented as $\chi_{H_2O}^{(2)}$ and $\chi_{H_2O}^{(3)}$) shown in (b). (c) Absolute net orientation of water (Θ) along the surface normal for different cation-containing solutions at various surface charges. Individual contributions from the first hydration shell (1st-H_2O), second hydration shell (2nd-H_2O), and non-hydrated water (non-H_2O) are considered. (d) Autocorrelation function of the residence time (eq S1), $R(t)$, for 1st-H_2O at a surface charge density of −35 mC/m^2. The number in parentheses is the half-life of 1st-H_2O around the corresponding cation. The half-life is defined as the time when half water molecules (marked by the red dashed line) leave the first hydration shell.

$\chi_{H_2O}^{(3)}$ term contains two parts: the second-order hyperpolarizability and the alignment of dipolar water by the interfacial electric field in the diffuse layer.[35,41] Our DFT calculations[23] have suggested that water polarization (dipole moment change due to charge redistribution by interfacial electric field) at Pt−water interfaces is almost independent of interfacial water structures, but the contribution from the water reorientation to the interfacial electric field is highly structural dependent. Therefore, the water dipole alignment should dominate $\chi_{H_2O}^{(3)}$. The $|\chi_{H_2O}^{(3)}|$ trend in the order of $K^+ > Li^+ > Ba^{2+}$ from Figure 2c suggests the water molecules in the diffuse layer cannot align to the interfacial electric field as efficiently when the cation−water interaction is strong, e.g., Ba^{2+}.

Molecular Dynamic Simulation. We carried out classical MD simulations to gain insights into the cation−water interactions at the Pt−water interface. We calculated the absolute water orientation (Figure S5, defined in eq S5) in the presence of K^+, Li^+, and Ba^{2+} at five surface charge densities (−15, −35, −42.5, −50, −60 mC/m^2) and then estimated the second-order optical susceptibility element, $\chi_{zzz}^{(2)}$, as a function of the surface potential ($\chi_{zzz}^{(2)}$ has previously been identified as the major SHG contributor at Pt−water interfaces under our experimental conditions[23]) from the orientation of interfacial water molecules[43]

$$\chi_{zzz}^{(2)}(z) = \sum_i \cos^3\theta_i(z)\delta[O_z(i) - z] \quad (5)$$

$$\chi_{zzz}^{(2)} = \int \chi_{zzz}^{(2)}(z)\mathrm{d}z \quad (6)$$

where $O_z(i)$ is the distance between the ith water (the oxygen atom) and the Pt surface. θ is the angle between the water orientation (defined by the sum of OH vectors) and the surface normal (Figure S5f).[44,45] As plotted in Figure 3a, $\chi_{zzz}^{(2)}$ increases when the surface potential becomes more negative regardless of the cation type. At the same potential, $\chi_{zzz}^{(2)}$ decreases in the order $K^+ > Li^+ > Ba^{2+}$. These findings are consistent with the experimental results in Figure 2b, suggesting that MD simulations can capture the interfacial water structure trend. We used eq 2 to fit data in Figure 3a for the potential-independent and -dependent susceptibilities, which are compared in Figure 3b (as water is assumed to be the sole contributor to the simulated $\chi_{zzz}^{(2)}$, we represent $\chi_S^{(2)}$ and $\chi_S^{(3)}$ as $\chi_{H_2O}^{(2)}$ and $\chi_{H_2O}^{(3)}$, respectively; see Table S4 for the fitted data). The obtained trends are qualitatively in agreement with the experimental results in Figure 2b, i.e., stronger cation−water interaction decreases both $\chi_{H_2O}^{(2)}$ and $\chi_{H_2O}^{(3)}$. Given the potential presence of chemisorbed water or hydroxyl species on Pt surfaces,[46,47] we performed additional simulations modeling water dissociative adsorption. As detailed in the Supporting Information (Section 4.3), our findings indicate that chemisorbed water or hydroxyl on Pt has a negligible impact on the distribution of ions and water molecules, and hence the simulated $\chi_{zzz}^{(2)}$ remains unaffected (Figure S10e).

We track how individual water structures contribute to the overall nonlinear optical response by counting contributions from water molecules of the first (1st-H_2O), the second (2nd-H_2O) hydration spheres, and the non-hydrated molecules (non-H_2O). The net water orientation value (Θ) of different hydration shells is decomposed using

https://doi.org/10.1021/jacs.3c09128
J. Am. Chem. Soc. XXXX, XXX, XXX−XXX

$$\Theta(z) = \sum_i \cos\theta_i(z)\delta[O_z(i) - z][H(r_{OM} - r_{O_iM}) \vee H(r_{OCl} - r_{O_iCl})] \quad (7)$$

$$\Theta = \int \Theta(z)dz \quad (8)$$

where r_{OM} and r_{OCl} are the cutoff distances between the water and ions (listed in Table S3); r_{O_iM} and r_{O_iCl} are the distances between the ith water and its nearest cation and Cl^- ion, respectively; H is the Heaviside function, and "$\vee$" is the "OR" operator.

The result of the analysis of the net water orientation is shown in Figure 3c. Regardless of the cation, non-H_2O contributes the most to Θ, followed by 2nd-H_2O and 1st-H_2O. The dominant role of non-H_2O is expected given that the number density of water is 2 orders of magnitude more than that of ions at the interface (see Figures S6 and S7). The contributions of 2nd-H_2O and 1st-H_2O are further diluted by the nature of the hydration shell, which tends to favor centrosymmetric configuration. The addition of surface charge increases the net water orientation (Θ) for all H_2O types, as water aligns to the interfacial electric field. The response of how Θ changes with the surface charge density (Figure S8) is weaker for hydrated water molecules compared to non-H_2O. This finding suggests that the water−cation interaction impedes the water reorientation in the EDL whereas non-H_2O is more labile and can facilely align to the EDL field polarization.

The type of cation strongly affects the competition between water−cation and water−field interactions. As plotted in Figure 3c, replacing K^+ with Li^+ or Ba^{2+} leads to a consistent decrease in Θ for all types of H_2O, irrespective of the surface charge density. We attribute this finding to the strength of the hydration shells: stronger cation−water interactions make it more difficult for the hydration water to align in response to interfacial polarization (which effectively lowers Θ).

We further track how the cation−water interaction can restrict the water movement. We calculated the residence time autocorrelation function $R(t)$ of a water molecule in the first hydration shell (Figure 3d, eq S1). We observed a faster decay of $R(t)$ with K^+ than with Li^+ and Ba^{2+}, and the 1st-H_2O half-life with Ba^{2+} is 20-fold longer than that with K^+, implying a more stable hydration shell with Ba^{2+}. Consequently, the water dipole alignment with K^+ is more susceptible to external perturbation than that with Ba^{2+} when the electrode surface charge is varied.

The interaction between cations and water has notable short- and long-range effects on the water orientation. For all ions at all charge densities, the water absolute orientation along the surface normal shows two featured regions (Figure S5). At $z < 1$ nm, ions accumulate near the surface (Figure S6), with an affinity of $Ba^{2+} > Li^+ > K^+$. Since ion adsorption in our simulation is driven by electrostatic forces, ions with high charge density should show higher affinity to the electrode.[44,48] Although the concentration of Ba^{2+} is only half of those of other ions, it has the highest affinity because of its bivalence. The conventional EDL model predicts the presence of a diffuse layer in which the absolute orientation of water decays exponentially. The profiles in Figure S5 at $z > 1.2$ nm with Li^+ and K^+ are consistent with this prediction, but for Ba^{2+}, it is difficult to conclude because water beyond 1.2 nm from the Pt surface shows no net orientation. In other words, the Ba^{2+} cations near the surface are so effective at screening the surface charges that the water molecules beyond even a nanometer away do not feel any electric fields from the electrode. In fact, when fitted to eq 2, $\chi_{zzz}^{(2)}$ of Ba^{2+} levels off at high surface charges (Figures 2b and 3a), unlike $\chi_{zzz}^{(2)}$ of Li^+ and K^+, which show a good linear correlation with the surface potential (Table S4). We attribute this finding to the excess Ba^{2+} adsorption at a high charge density surfaces, whose impact on the interfacial water structure is different vs K^+ or even Li^+. This charge compensation mechanism is different from previous observations with localized surface charges, where adsorption of excess counterions leads to charge over-compensating and even reversing the electric fields and water net orientations in the diffuse layer.[25,44,48−50] Such intricate details of the short- and long-range interactions at electrode−electrolyte interfaces (especially with the presence of high-valent cations) are difficult to describe by classical EDL theory models.

The Effect of Cations on Interfacial Water Structures and the Implications for HER. We can summarize the insights from our SHG and MD studies as follows (Figure 4a): strongly hydrated cations like Ba^{2+} reduce the net orientation of nearby water (1) by preserving a centrosymmetric hydration sphere and (2) by providing more effective screening (i.e., water network becomes more disordered along the electrode surface normal), and (3) makes the nearby H_2O more difficult to realign with the EDL field (i.e., water molecules become less polarizable).

This newfound information has implications for our understanding of the cation effect on Pt HER. The first one is the positive shift of H_{upd} peaks in the presence of more weakly hydrated cations (Figure 1a).[7,29,30] The traditional view that H_{upd} refers to the ad- and desorption of hydrogen has recently been challenged by Koper and Janik,[51−53] who suggest this peak results from the exchange of proton with surface-bound hydroxyl species (OH*) on Pt, as represented by

$$OH^* + H_2O + 2e^- \leftrightarrow 2OH^- + H^* \quad (9)$$

Considering our observation that cations strongly affect interfacial water structures, we can explain the cation effect on H_{upd} through the following mechanism (Figure 4b): weakly hydrated cations, owing to its loose hydration shell, interact with OH* more facilely to form a transient cation−OH^- ion pair. This interaction allows OH* to be more readily displaced by H* (causing it to shift to a more positive potential). This explanation is also consistent with the H*/OH* exchange kinetics observed from CV studies[29] that eq 9 is faster in KOH than in LiOH, as the hydration shell of K^+ is more labile than that of Li^+ (Figure 3d).

We next discuss the cation effect on Pt HER kinetics, i.e., why does the presence of Li^+ benefit alkaline HER kinetics?[6,54] The formation of the adsorbed hydrogen, or Volmer step, is recognized as the rate-determining step in Pt alkaline HER,[55,56] which is represented below

$$\text{Volmer step: } H_2O + e^- + {}^* \rightarrow H^* + OH^- \quad (10)$$

Given that water serves as the proton source for H* in alkaline water and our SHG and MD results suggest cations modifying the interfacial water, we propose here a cation hydration-mediated mechanism for the Volmer step (Figure 4c). For simplicity, we will represent water that has been

https://doi.org/10.1021/jacs.3c09128
J. Am. Chem. Soc. XXXX, XXX, XXX−XXX

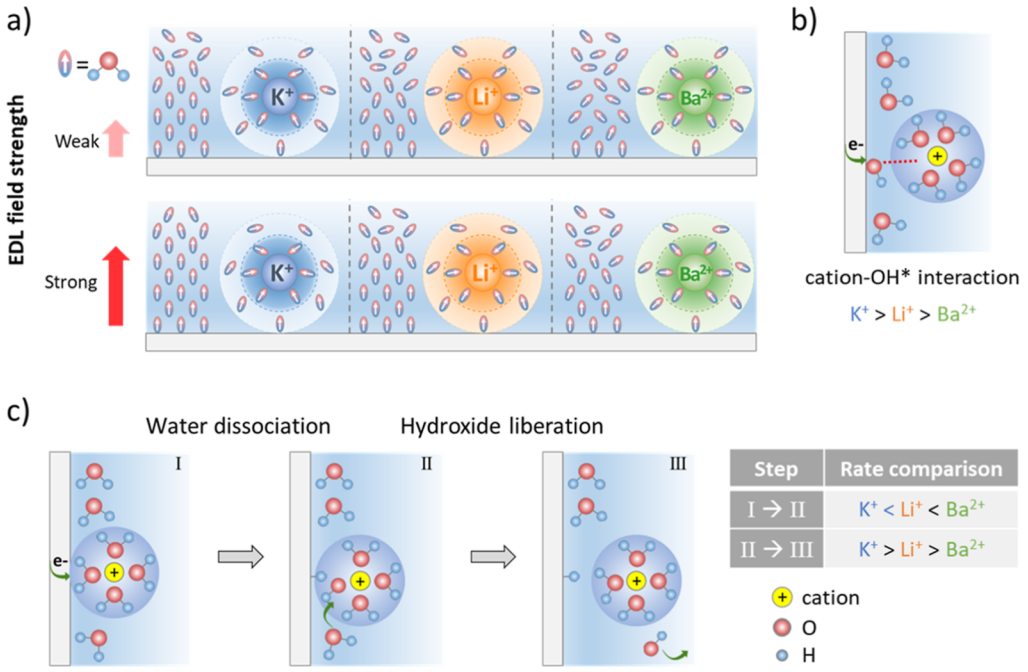

Figure 4. Schematic illustration of the cation effects on (a) the dipole distribution of non-H_2O, 1st-H_2O, and 2nd-H_2O at electrode surfaces, (b) the cation−OH* interaction weakening OH* binding, and (c) the rate of cation hydration-mediated HER Volmer steps. The water dissociation step (I → II) and the hydroxide liberation step (II → III) correspond to eqs 11 and 12, respectively.

modified by a cation as $M(H_2O)x$ (M and x represent cation and the water coordination number, respectively; the cation charge is omitted for clarity). When the electrode surface is negatively charged, cations are attracted toward the electrode surface and enter into the inner Helmholtz plane (Figure 4c-I), bringing with them H_2O. We hypothesize that the presence of a cation affects water dissociation at the interface, forming H* at the electrode surface and leaving behind OH^- (Figure 4c-II, eq 11). OH^- is then free to exchange with a non-H_2O nearby to regenerate the water molecules for the next Volmer cycle (Figure 4c-III, eq 12).

$$\text{Water dissociation: } M(H_2O)_x + e^- + {}^* \rightarrow H^* + M(H_2O)_{x-1}(OH^-) \quad (11)$$

$$\text{Hydroxide liberation: } M(H_2O)_{x-1}(OH^-) + H_2O \rightarrow M(H_2O)_x + OH^- \quad (12)$$

Using the above hypothesis, we can rationalize the kinetic trend in Figure 1b. The water dissociation in eq 11 correlates with the pK_a of hydrated water, which is lower with cations of higher hydration energy (K^+: 14.0, Li^+: 13.6, Ba^{2+}: 13.4[57]). Therefore, we expect eq 11 to be more facile in the presence of $Ba^{2+} > Li^+ > K^+$. After this step, OH^- liberating from the hydration shell occurs by exchanging with a nearby non-H_2O as shown in eq 12. However, OH^- as a hard Lewis base prefers to interact with a hard Lewis acid (with the hardness increasing in the order of $K^+ < Li^+ < Ba^{2+}$), as indicated by the lattice energy trend of $Ba(OH)_2 > LiOH > KOH$ and the solubility trend in water of $Ba(OH)_2 < LiOH < KOH$.[58] One thus expects the rate of eq 12 to be faster with K^+ and slower with Ba^{2+}. The best HER kinetics is therefore realized in Li^+ (Figure 1b), where the balance between water dissociation (eq 11) and hydrated OH^- liberation (eq 12) is optimal. This idea of cations mediating the water dissociation in the Volmer step is in line with recent ab initio molecular dynamics simulations.[14] Future tests of the above hypothesis of how cation−water interactions can affect HER kinetics (e.g., by monitoring the interfacial water structure in the presence of the cations during the reaction turnover) would be an essential step toward validating the presented theory.

CONCLUSIONS

We report how cations (Ba^{2+}, Li^+, and K^+) affect interfacial water structures in alkaline media using in situ PS-SHG measurements and classical MD simulations. We extracted the nonlinear optical susceptibilities for interfacial water, $\chi^{(2)}_{H_2O}$ and $\chi^{(3)}_{H_2O}$, whose magnitude showed a trend of $K^+ > Li^+ > Ba^{2+}$. This observation indicates that the net orientation of interfacial water and its ability to reorient to the EDL field decrease in the presence of strongly hydrated cations. These interpretations are supported by classical MD simulations, where the experimental trends of $\chi^{(2)}_{H_2O}$ and $\chi^{(3)}_{H_2O}$ can be reproduced by solely considering water molecule orientations. By analyzing water molecules of different hydration states (1st-H_2O, 2nd-H_2O, and non-H_2O), we found that their net orientation is a balance between water−cation and water−field interactions. In other words, while a higher surface charge density can increase water net orientations through polarization, this effect is countered by strong cation−water interactions. We also showed that water molecules become less labile when they interact with cations of higher hydration energy. With these new insights, we explained the cation effect on the H_{upd} peak positions by considering the rigidity of cation hydration spheres. For the cation-dependent kinetics of Pt alkaline HER, we proposed a cation hydration-mediated mechanism for the Volmer step, which involves the dissociation of hydrated water and the regeneration of the hydration shell. Overall, our study shows that the cation modifies the structure of interfacial water

https://doi.org/10.1021/jacs.3c09128
J. Am. Chem. Soc. XXXX, XXX, XXX−XXX

molecules and highlights the strategy of using additives to the interfacial water layer and local environment in electrocatalysis.

■ ASSOCIATED CONTENT

Supporting Information

The Supporting Information is available free of charge at https://pubs.acs.org/doi/10.1021/jacs.3c09128.

Experimental details including electrode preparation, electrochemical, and SHG measurements. Simulation details. Discussion on the SHG response at Pt−water interfaces. Simulated water and ion distribution near the Pt electrode (PDF)

■ AUTHOR INFORMATION

Corresponding Authors

Pengtao Xu − *Department of Materials Science and Engineering, Cornell University, Ithaca, New York 14850, United States;* Present Address: In Situ Center for Physical Sciences, School of Chemistry and Chemical Engineering, Shanghai Jiao Tong University, Shanghai, 200240, China; orcid.org/0000-0002-4470-446X; Email: xupengtao@sjtu.edu.cn

Jin Suntivich − *Department of Materials Science and Engineering, Cornell University, Ithaca, New York 14850, United States; Kavli Institute at Cornell for Nanoscale Science, Cornell University, Ithaca, New York 14850, United States;* orcid.org/0000-0002-3427-4363; Email: jsuntivich@cornell.edu

Authors

Ruiyu Wang − *Department of Chemistry, Temple University, Philadelphia, Pennsylvania 19122, United States; Center for Complex Materials from First-Principles (CCM), Temple University, Philadelphia, Pennsylvania 19122, United States;* orcid.org/0000-0003-1608-140X

Haojian Zhang − *Department of Materials Science and Engineering, Cornell University, Ithaca, New York 14850, United States*

Vincenzo Carnevale − *Institute for Computational Molecular Science and Department of Biology, Temple University, Philadelphia, Pennsylvania 19122, United States;* orcid.org/0000-0002-1918-8280

Eric Borguet − *Department of Chemistry, Temple University, Philadelphia, Pennsylvania 19122, United States; Center for Complex Materials from First-Principles (CCM), Temple University, Philadelphia, Pennsylvania 19122, United States;* orcid.org/0000-0003-0593-952X

Complete contact information is available at: https://pubs.acs.org/10.1021/jacs.3c09128

Author Contributions

▽P.X. and R.W. made equal contributions.

Notes

The authors declare no competing financial interest.

■ ACKNOWLEDGMENTS

This work was supported as part of the Center for Alkaline Based Energy Solutions, an Energy Frontier Research Center funded by the US Department of Energy (DOE), Office of Science, Office of Basic Energy Sciences under award #DE-SC0019445 (electrochemistry and spectroscopy). This work made use of the Cornell Center for Materials Research Shared Facilities which are supported through the NSF MRSEC program (DMR-1719875). The simulation work was supported as part of the Center for Complex Materials from First-Principles (CCM), an Energy Frontier Research Center funded by the U.S. Department of Energy, Office of Science, Basic Energy Sciences under award #DE-SC0012575. The computational work was performed on Temple University's HPC resources supported in part by the National Science Foundation through major research instrumentation grant number 1625061 and by the US Army Research Laboratory under contract number W911NF-16-2-0189. R.W., V.C., and E.B. acknowledge the support from National Science Foundation (CHE 2102557) for the theoretical simulation part.

■ REFERENCES

(1) Seh, Z. W.; Kibsgaard, J.; Dickens, C. F.; Chorkendorff, I.; Nørskov, J. K.; Jaramillo, T. F. Combining Theory and Experiment in Electrocatalysis: Insights into Materials Design. *Science* **2017**, *355* (6321), No. eaad4998.

(2) Stamenkovic, V. R.; Strmcnik, D.; Lopes, P. P.; Markovic, N. M. Energy and Fuels from Electrochemical Interfaces. *Nat. Mater.* **2017**, *16* (1), 57−69.

(3) Waegele, M. M.; Gunathunge, C. M.; Li, J.; Li, X. How Cations Affect the Electric Double Layer and the Rates and Selectivity of Electrocatalytic Processes. *J. Chem. Phys.* **2019**, *151* (16), 160902.

(4) Rebollar, L.; Intikhab, S.; Oliveira, N. J.; Yan, Y.; Xu, B.; McCrum, I. T.; Snyder, J. D.; Tang, M. H. Beyond Adsorption" Descriptors in Hydrogen Electrocatalysis. *ACS Catal.* **2020**, *10* (24), 14747−14762.

(5) Marcandalli, G.; Monteiro, M. C. O.; Goyal, A.; Koper, M. T. M. Electrolyte Effects on CO2 Electrochemical Reduction to CO. *Acc. Chem. Res.* **2022**, *55* (14), 1900−1911.

(6) Huang, B.; Rao, R. R.; You, S.; Hpone Myint, K.; Song, Y.; Wang, Y.; Ding, W.; Giordano, L.; Zhang, Y.; Wang, T.; Muy, S.; Katayama, Y.; Grossman, J. C.; Willard, A. P.; Xu, K.; Jiang, Y.; Shao-Horn, Y. Cation- and pH-Dependent Hydrogen Evolution and Oxidation Reaction Kinetics. *JACS Au* **2021**, *1* (10), 1674−1687.

(7) Liu, E.; Li, J.; Jiao, L.; Doan, H. T. T.; Liu, Z.; Zhao, Z.; Huang, Y.; Abraham, K. M.; Mukerjee, S.; Jia, Q. Unifying the Hydrogen Evolution and Oxidation Reactions Kinetics in Base by Identifying the Catalytic Roles of Hydroxyl-Water-Cation Adducts. *J. Am. Chem. Soc.* **2019**, *141* (7), 3232−3239.

(8) Strmcnik, D.; Kodama, K.; van der Vliet, D.; Greeley, J.; Stamenkovic, V. R.; Marković, N. M. The Role of Non-Covalent Interactions in Electrocatalytic Fuel-Cell Reactions on Platinum. *Nat. Chem.* **2009**, *1* (6), 466−472.

(9) Rao, R. R.; Huang, B.; Katayama, Y.; Hwang, J.; Kawaguchi, T.; Lunger, J. R.; Peng, J.; Zhang, Y.; Morinaga, A.; Zhou, H.; You, H.; Shao-Horn, Y. pH- and Cation-Dependent Water Oxidation on Rutile RuO 2 (110). *J. Phys. Chem. C* **2021**, *125* (15), 8195−8207.

(10) Ringe, S.; Clark, E. L.; Resasco, J.; Walton, A.; Seger, B.; Bell, A. T.; Chan, K. Understanding Cation Effects in Electrochemical CO2 Reduction. *Energy Environ. Sci.* **2019**, *12* (10), 3001−3014.

(11) Ringe, S.; Morales-Guio, C. G.; Chen, L. D.; Fields, M.; Jaramillo, T. F.; Hahn, C.; Chan, K. Double Layer Charging Driven Carbon Dioxide Adsorption Limits the Rate of Electrochemical Carbon Dioxide Reduction on Gold. *Nat. Commun.* **2020**, *11* (1), 33.

(12) Monteiro, M. C. O.; Dattila, F.; López, N.; Koper, M. T. M. The Role of Cation Acidity on the Competition between Hydrogen Evolution and CO 2 Reduction on Gold Electrodes. *J. Am. Chem. Soc.* **2022**, *144* (4), 1589−1602.

(13) Monteiro, M. C. O.; Goyal, A.; Moerland, P.; Koper, M. T. M. Understanding Cation Trends for Hydrogen Evolution on Platinum and Gold Electrodes in Alkaline Media. *ACS Catal.* **2021**, *11*, 14328−14335.

(14) Wang, Y.-H.; Zheng, S.; Yang, W.-M.; Zhou, R.-Y.; He, Q.-F.; Radjenovic, P.; Dong, J.-C.; Li, S.; Zheng, J.; Yang, Z.-L.; Attard, G.; Pan, F.; Tian, Z.-Q.; Li, J.-F. In Situ Raman Spectroscopy Reveals the Structure and Dissociation of Interfacial Water. *Nature* **2021**, *600* (7887), 81−85.
(15) Dubouis, N.; Serva, A.; Salager, E.; Deschamps, M.; Salanne, M.; Grimaud, A. The Fate of Water at the Electrochemical Interfaces: Electrochemical Behavior of Free Water Versus Coordinating Water. *J. Phys. Chem. Lett.* **2018**, *9* (23), 6683−6688.
(16) Rozsa, V.; Pham, T. A.; Galli, G. Molecular Polarizabilities as Fingerprints of Perturbations to Water by Ions and Confinement. *J. Chem. Phys.* **2020**, *152* (12), 124501.
(17) Dalstein, L.; Chiang, K.-Y.; Wen, Y.-C. Direct Quantification of Water Surface Charge by Phase-Sensitive Second Harmonic Spectroscopy. *J. Phys. Chem. Lett.* **2019**, *10* (17), 5200−5205.
(18) Nahalka, I.; Zwaschka, G.; Campen, R. K.; Marchioro, A.; Roke, S. Mapping Electrochemical Heterogeneity at Gold Surfaces: A Second Harmonic Imaging Study. *J. Phys. Chem. C* **2020**, *124* (37), 20021−20034.
(19) Ma, E.; Geiger, F. M. Divalent Ion Specific Outcomes on Stern Layer Structure and Total Surface Potential at the Silica:Water Interface. *J. Phys. Chem. A* **2021**, *125* (46), 10079−10088.
(20) Ohno, P. E.; Chang, H.; Spencer, A. P.; Liu, Y.; Boamah, M. D.; Wang, H.; Geiger, F. M. Beyond the Gouy-Chapman Model with Heterodyne-Detected Second Harmonic Generation. *J. Phys. Chem. Lett.* **2019**, *10* (10), 2328−2334.
(21) Shen, Y. R. Surface Properties Probed by Second-Harmonic and Sum-Frequency Generation. *Nature* **1989**, *337* (6207), 519−525.
(22) Xu, P.; Huang, A.; Suntivich, J. Phase-Sensitive Second-Harmonic Generation of Electrochemical Interfaces. *J. Phys. Chem. Lett.* **2020**, *11* (19), 8216−8221.
(23) Xu, P.; von Rueden, A. D.; Schimmenti, R.; Mavrikakis, M.; Suntivich, J. Optical Method for Quantifying the Potential of Zero Charge at the Platinum-Water Electrochemical Interface. *Nat. Mater.* **2023**, *22* (4), 503−510.
(24) Piontek, S. M.; DelloStritto, M.; Mandal, B.; Marshall, T.; Klein, M. L.; Borguet, E. Probing Heterogeneous Charge Distributions at the α-Al2O3(0001)/H2O Interface. *J. Am. Chem. Soc.* **2020**, *142* (28), 12096−12105.
(25) Wang, R.; Klein, M. L.; Carnevale, V.; Borguet, E. Investigations of Water/Oxide Interfaces by Molecular Dynamics Simulations. *Wiley Interdiscip. Rev.: Comput. Mol. Sci.* **2021**, *11* (6), No. e1537.
(26) Bedrov, D.; Piquemal, J.-P.; Borodin, O.; MacKerell, A. D.; Roux, B.; Schröder, C. Molecular Dynamics Simulations of Ionic Liquids and Electrolytes Using Polarizable Force Fields. *Chem. Rev.* **2019**, *119* (13), 7940−7995.
(27) Alfarano, S. R.; Pezzotti, S.; Stein, C. J.; Lin, Z.; Sebastiani, F.; Funke, S.; Hoberg, C.; Kolling, I.; Ma, C. Y.; Mauelshagen, K.; Ockelmann, T.; Schwaab, G.; Fu, L.; Brubach, J.-B.; Roy, P.; Head-Gordon, M.; Tschulik, K.; Gaigeot, M.-P.; Havenith, M. Stripping Away Ion Hydration Shells in Electrical Double-Layer Formation: Water Networks Matter. *Proc. Natl. Acad. Sci. U.S.A.* **2021**, *118* (47), No. e2108568118.
(28) Kann, Z. R.; Skinner, J. L. A Scaled-Ionic-Charge Simulation Model That Reproduces Enhanced and Suppressed Water Diffusion in Aqueous Salt Solutions. *J. Chem. Phys.* **2014**, *141* (10), 104507.
(29) Intikhab, S.; Snyder, J. D.; Tang, M. H. Adsorbed Hydroxide Does Not Participate in the Volmer Step of Alkaline Hydrogen Electrocatalysis. *ACS Catal.* **2017**, *7* (12), 8314−8319.
(30) Chen, X.; McCrum, I. T.; Schwarz, K. A.; Janik, M. J.; Koper, M. T. M. Co-Adsorption of Cations as the Cause of the Apparent pH Dependence of Hydrogen Adsorption on a Stepped Platinum Single-Crystal Electrode. *Angew. Chem., Int. Ed.* **2017**, *56* (47), 15025−15029.
(31) Sheng, W.; Gasteiger, H. A.; Shao-Horn, Y. Hydrogen Oxidation and Evolution Reaction Kinetics on Platinum: Acid vs Alkaline Electrolytes. *J. Electrochem. Soc.* **2010**, *157* (11), B1529.
(32) Ojha, K.; Doblhoff-Dier, K.; Koper, M. T. M. Double-Layer Structure of the Pt(111)-Aqueous Electrolyte Interface. *Proc. Natl. Acad. Sci. U.S.A.* **2022**, *119* (3), No. e2116016119.
(33) Krause, D.; Teplin, C. W.; Rogers, C. T. Optical Surface Second Harmonic Measurements of Isotropic Thin-Film Metals: Gold, Silver, Copper, Aluminum, and Tantalum. *J. Appl. Phys.* **2004**, *96* (7), 3626−3634.
(34) Ma, E.; Kim, J.; Chang, H.; Ohno, P. E.; Jodts, R. J.; Miller, T. F.; Geiger, F. M. Stern and Diffuse Layer Interactions during Ionic Strength Cycling. *J. Phys. Chem. C* **2021**, *125* (32), 18002−18014.
(35) Boamah, M. D.; Ohno, P. E.; Lozier, E.; Van Ardenne, J.; Geiger, F. M. Specifics about Specific Ion Adsorption from Heterodyne-Detected Second Harmonic Generation. *J. Phys. Chem. B* **2019**, *123* (27), 5848−5856.
(36) Xu, M.; Spinney, R.; Allen, H. C. Water Structure at the Air-Aqueous Interface of Divalent Cation and Nitrate Solutions. *J. Phys. Chem. B* **2009**, *113* (13), 4102−4110.
(37) Flores, S. C.; Kherb, J.; Konelick, N.; Chen, X.; Cremer, P. S. The Effects of Hofmeister Cations at Negatively Charged Hydrophilic Surfaces. *J. Phys. Chem. C* **2012**, *116* (9), 5730−5734.
(38) Lovering, K. A.; Bertram, A. K.; Chou, K. C. New Information on the Ion-Identity-Dependent Structure of Stern Layer Revealed by Sum Frequency Generation Vibrational Spectroscopy. *J. Phys. Chem. C* **2016**, *120* (32), 18099−18104.
(39) Nihonyanagi, S.; Yamaguchi, S.; Tahara, T. Counterion Effect on Interfacial Water at Charged Interfaces and Its Relevance to the Hofmeister Series. *J. Am. Chem. Soc.* **2014**, *136* (17), 6155−6158.
(40) Hunger, J.; Schaefer, J.; Ober, P.; Seki, T.; Wang, Y.; Prädel, L.; Nagata, Y.; Bonn, M.; Bonthuis, D. J.; Backus, E. H. G. Nature of Cations Critically Affects Water at the Negatively Charged Silica Interface. *J. Am. Chem. Soc.* **2022**, *144* (43), 19726−19738.
(41) Ong, S.; Zhao, X.; Eisenthal, K. B. Polarization of Water Molecules at a Charged Interface: Second Harmonic Studies of the Silica/Water Interface. *Chem. Phys. Lett.* **1992**, *191* (3−4), 327−335.
(42) Le Breton, G.; Bonhomme, O.; Benichou, E.; Loison, C. First Hyperpolarizability of Water in Bulk Liquid Phase: Long-Range Electrostatic Effects Included via the Second Hyperpolarizability. *Phys. Chem. Chem. Phys.* **2022**, *24* (32), 19463−19472.
(43) Eisenthal, K. B. Equilibrium and Dynamic Processes at Interfaces by Second Harmonic and Sum Frequency Generation. *Annu. Rev. Phys. Chem.* **1992**, *43* (1), 627−661.
(44) Wang, R.; DelloStritto, M.; Remsing, R. C.; Carnevale, V.; Klein, M. L.; Borguet, E. Sodium Halide Adsorption and Water Structure at the α-Alumina(0001)/Water Interface. *J. Phys. Chem. C* **2019**, *123* (25), 15618−15628.
(45) Wang, R.; Zou, Y.; Remsing, R. C.; Ross, N. O.; Klein, M. L.; Carnevale, V.; Borguet, E. Superhydrophilicity of α -Alumina Surfaces Results from Tight Binding of Interfacial Waters to Specific Aluminols. *J. Colloid Interface Sci.* **2022**, *628*, 943−954.
(46) Clavilier, J.; Albalat, R.; Gomez, R.; Orts, J. M.; Feliu, J. M.; Aldaz, A. Study of the Charge Displacement at Constant Potential during CO Adsorption on Pt(110) and Pt(111) Electrodes in Contact with a Perchloric Acid Solution. *J. Electroanal. Chem.* **1992**, *330* (1−2), 489−497.
(47) Rizo, R.; Fernández-Vidal, J.; Hardwick, L. J.; Attard, G. A.; Vidal-Iglesias, F. J.; Climent, V.; Herrero, E.; Feliu, J. M. Investigating the Presence of Adsorbed Species on Pt Steps at Low Potentials. *Nat. Commun.* **2022**, *13* (1), 2550.
(48) Dewan, S.; Carnevale, V.; Bankura, A.; Eftekhari-Bafrooei, A.; Fiorin, G.; Klein, M. L.; Borguet, E. Structure of Water at Charged Interfaces: A Molecular Dynamics Study. *Langmuir* **2014**, *30* (27), 8056−8065.
(49) Burt, R.; Birkett, G.; Zhao, X. S. A Review of Molecular Modelling of Electric Double Layer Capacitors. *Phys. Chem. Chem. Phys.* **2014**, *16* (14), 6519−6538.
(50) Piontek, S. M.; Tuladhar, A.; Marshall, T.; Borguet, E. Monovalent and Divalent Cations at the α-Al2O3(0001)/Water Interface: How Cation Identity Affects Interfacial Ordering and

https://doi.org/10.1021/jacs.3c09128
J. Am. Chem. Soc. XXXX, XXX, XXX−XXX

Vibrational Dynamics. *J. Phys. Chem. C* **2019**, *123* (30), 18315−18324.
(51) van der Niet, M. J. T. C.; Garcia-Araez, N.; Hernández, J.; Feliu, J. M.; Koper, M. T. M. Water Dissociation on Well-Defined Platinum Surfaces: The Electrochemical Perspective. *Catal. Today* **2013**, *202* (1), 105−113.
(52) McCrum, I. T.; Janik, M. J. pH and Alkali Cation Effects on the Pt Cyclic Voltammogram Explained Using Density Functional Theory. *J. Phys. Chem. C* **2016**, *120* (1), 457−471.
(53) Janik, M. J.; McCrum, I. T.; Koper, M. T. M. On the Presence of Surface Bound Hydroxyl Species on Polycrystalline Pt Electrodes in the "Hydrogen Potential Region" (0−0.4 V-RHE). *J. Catal.* **2018**, *367*, 332−337.
(54) Subbaraman, R.; Tripkovic, D.; Strmcnik, D.; Chang, K. C. K.-C.; Uchimura, M.; Paulikas, A. P.; Stamenkovic, V.; Markovic, N. M. Enhancing Hydrogen Evolution Activity in Water Splitting by Tailoring Li+-Ni(OH)2-Pt Interfaces. *Science* **2011**, *334* (6060), 1256−1260.
(55) Rheinländer, P. J.; Herranz, J.; Durst, J.; Gasteiger, H. A. Kinetics of the Hydrogen Oxidation/Evolution Reaction on Polycrystalline Platinum in Alkaline Electrolyte Reaction Order with Respect to Hydrogen Pressure. *J. Electrochem. Soc.* **2014**, *161* (14), F1448−F1457.
(56) McCrum, I. T.; Koper, M. T. M. M. The Role of Adsorbed Hydroxide in Hydrogen Evolution Reaction Kinetics on Modified Platinum. *Nat. Energy* **2020**, *5* (11), 891−899.
(57) Hawkes, S. J. All Positive Ions Give Acid Solutions in Water. *J. Chem. Educ.* **1996**, *73* (6), 516−517.
(58) Haynes, W. M. *CRC Handbook of Chemistry and Physics*. 95th ed.; CRC Press: Boca Raton, 2014; p 2704; .

https://doi.org/10.1021/jacs.3c09128
J. Am. Chem. Soc. XXXX, XXX, XXX−XXX